

The Lord of the Ring Road: A Review and Evaluation of Autonomous Control Policies for Traffic in a Ring Road

FANG-CHIEH CHOU, ALBEN ROME BAGABALDO, and ALEXANDRE M. BAYEN,
UC Berkeley

This study focuses on the comprehensive investigation of stop-and-go waves appearing in closed-circuit ring road traffic wherein we evaluate various longitudinal dynamical models for vehicles. It is known that the behavior of human-driven vehicles, with other traffic elements such as density held constant, could stimulate stop-and-go waves, which do not dissipate on the circuit ring road. Stop-and-go waves can be dissipated by adding automated vehicles (AVs) to the ring. Thorough investigations of the performance of AV longitudinal control algorithms were carried out in Flow, which is an integrated platform for reinforcement learning on traffic control. Ten AV algorithms presented in the literature are evaluated. For each AV algorithm, experiments are carried out by varying distributions and penetration rates of AVs. Two different distributions of AVs are studied. For the first distribution scenario, AVs are placed consecutively. Penetration rates are varied from 1 AV (5%) to all AVs (100%). For the second distribution scenario, AVs are placed with even distribution of human-driven vehicles in between any two AVs. In this scenario, penetration rates are varied from 2 AVs (10%) to 11 AVs (50%). Multiple runs (10 runs) are simulated to average out the randomness in the results. From more than 3,000 simulation experiments, we investigated how AV algorithms perform differently with varying distributions and penetration rates while all AV algorithms remained fixed under all distributions and penetration rates. Time to stabilize, maximum headway, vehicle miles traveled, and fuel economy are used to evaluate their performance. Using these metrics, we find that the traffic condition improvement is not necessarily dependent on the distribution for most of the AV controllers, particularly when no cooperation among AVs is considered. Traffic condition is generally improved with a higher AV penetration rate with only one of the AV algorithms showing a contrary trend. Among all AV algorithms in this study, the reinforcement learning controller shows the most consistent improvement under all distributions and penetration rates.

CCS Concepts: • **General and reference** → **Surveys and overviews**; • **Computing methodologies** → **Reinforcement learning; Modeling and simulation**;

With code contributions from (alphabetically by last name): RAHUL BHADANI (The University of Arizona), MARIA-LAURA DELLE MONACHE (Inria Research Centre Grenoble Rhône-Alpes), ABDUL RAHMAN KREIDIEH (UC Berkeley), BENEDETTO PICCOLI (Rutgers University Camden), JONATHAN SPRINKLE (The University of Arizona), EUGENE VINITSKY (UC Berkeley), and CATHY WU (MIT).

This material is based upon work supported by the National Science Foundation under Grant Numbers CNS-1837244 (A. Bayen), CNS-1837652 (D. Work), CNS-1837481 (B. Piccoli), CNS-1446435 (J. Sprinkle). Any opinions, findings, and conclusions or recommendations expressed in this material are those of the author(s) and do not necessarily reflect the views of the National Science Foundation. This material is based upon work supported by the U.S. Department of Energy's Office of Energy Efficiency and Renewable Energy (EERE) award number CID DE-EE0008872. The views expressed herein do not necessarily represent the views of the U.S. Department of Energy or the United States Government.

Authors' address: F.-C. Chou, A. R. Bagabaldo, and A. M. Bayen, UC Berkeley, P.O. Box 1212, Berkeley, California, 94709; emails: {fcchou, bagabaldo, bayen}@berkeley.edu.

Permission to make digital or hard copies of all or part of this work for personal or classroom use is granted without fee provided that copies are not made or distributed for profit or commercial advantage and that copies bear this notice and the full citation on the first page. Copyrights for components of this work owned by others than ACM must be honored. Abstracting with credit is permitted. To copy otherwise, or republish, to post on servers or to redistribute to lists, requires prior specific permission and/or a fee. Request permissions from permissions@acm.org.

© 2022 Association for Computing Machinery.

2378-962X/2022/01-ART8 \$15.00

<https://doi.org/10.1145/3494577>

Additional Key Words and Phrases: Automated vehicle, reinforcement learning, ring road, car-following model

ACM Reference format:

Fang-Chieh Chou, Alben Rome Bagabaldo, and Alexandre M. Bayen. 2022. The Lord of the Ring Road: A Review and Evaluation of Autonomous Control Policies for Traffic in a Ring Road. *ACM Trans. Cyber-Phys. Syst.* 6, 1, Article 8 (January 2022), 25 pages. <https://doi.org/10.1145/3494577>

1 INTRODUCTION

“One ring to rule them all,” *The Lord of the Rings*, J. R. R. Tolkien (1954) [38]. The future of traffic autonomy lands to the power of the *Ring*.

This study focuses on a comprehensive investigation of a special traffic phenomenon appearing on closed-circuit ring roads wherein despite the fact that everything else is held constant (i.e., the number of vehicles are kept the same with unchanged road dimensions), stop-and-go waves propagate upstream against the flow of traffic and travel backward along the road, creating so-called phantom congestion. This article studies the ring road with fundamental mathematical equations describing **car-following models (CFMs)** and discusses results from other researchers with a thorough literature survey. Studying this traffic phenomenon on the ring road yields insights about occurrences of traffic jams that also appear on an open straight road [18, 43] from which congestion mitigation strategies can be derived.

CFMs are used to describe driving behavioral patterns of **human-driven vehicles (HVs)** and are considered to be the most important representatives of microscopic traffic flow models in studying traffic behavior to address congestion [40]. The early works in developing CFMs date back to the 1950s. The first two researchers who are known to introduce dynamical elements of a line of vehicles are Reuschel [32] in 1950 and Pipes [29] in 1953. In their works, they were able to include an important element of modern microscopic modeling: the safety distance between vehicles (i.e., minimum bumper-to-bumper distance of a vehicle following a leading vehicle). Their models focus on the dynamical behavior of a stream of vehicles as they accelerate or decelerate and as each leader-follower pair follows each other, making it a foundation among the most recent advances in CFMs. There are many other researchers who extended the works of Reuschel and Pipes. Among them are Kometani and Sasaki [17] in 1958 and Herman et al. [14] at General Motors. These early works were called *minimal models* because they are “not complete and can’t describe either free traffic or approaches to standing obstacles” [40, Chapter 10].

It was more challenging to solve for time-continuous models because they tended to be highly computationally expensive in the earlier years. To compensate for this, discrete-time models were developed. One of the arguably simplest discrete-time models is the CFM of Newell [27], which considers that a leading vehicle is following a preceding vehicle on a homogeneous highway, and the time-space trajectory of the leading vehicle is assumed to be the same as the preceding vehicle. Along the traffic wave speed, the leading vehicle changes its speed based on the preceding vehicle at any time-space point. However, the advancements in computing technologies have allowed the use of time-continuous models to be more feasible and flexible. The popularity of time-continuous models, like the **intelligent driver model (IDM)**, which according to Treiber and Kesting [40, Chapter 11] is “probably the simplest, complete and accident-free model producing realistic acceleration profiles and a plausible behavior in essentially all single-lane traffic situations,” making them widely applied and adopted in traffic modeling and vehicle controller design.

Since the early 1990s, numerous researchers have demonstrated traffic congestion without bottlenecks in closed networks. Nagel and Schreckenberg [26] showed spontaneous traffic jams on a closed ring road with a cellular automaton model. Sugiyama et al. [35] experimentally showed the so-called phantom traffic jam phenomenon on a closed-circuit road. Tadaki et al. [37] also demonstrated stop-and-go waves on a ring road with a similar real-world experimental setup. Various numbers of vehicles on rings with different ring radii were experimented. They showed that critical density for emergence of traffic jam is consistent with critical density found on a real highway.

The emergence of **automated vehicles (AVs)** was pushed forward when the Defense Advanced Research Projects Agency, the research arm of the U.S. Department of Defense, organized a series of challenges in 2004–2013. This interest for AVs grew further when Tesla's Autopilot was launched in 2014. Transportation network companies like Uber and Lyft are also now invested in research for autonomous cars. It is expected that AVs have the potential to improve not only safety [10, 24, 42] but also efficiency [1, 41] and mobility [7, 46]. The idea of using AVs to stabilize stop-and-go waves on a ring road had been studied. The emergence of stop-and-go waves on a ring road can be viewed as instability of a dynamical system. Theoretically, the ring road is not controllable, but it is stabilizable [44]. Therefore, the ring road can be stabilized with an AV as a state feedback controller, although a full state feedback controller may not necessarily be needed for stabilizing the system. The dynamics of the ring road can be totally different by replacing a HV with an AV, and so can the stability. If the AV model is selected carefully, the ring road stability may be achieved even without a full state feedback controller. Cui et al. [6] carried out a stability analysis and showed the possibility of smoothing traffic flow with a single AV on a ring road in the simulation. Stern et al. [34] verified the idea of smoothing traffic on a ring road. Horn et al. [15] proposed a bilateral controller to stabilize the ring road traffic. Wu et al. [48] used the **reinforcement learning (RL)** controller to stabilize ring road traffic. Delle Monache et al. [8] proposed a Lyapunov-based controller for dissipating traffic waves and validated it on the ring road. Zheng et al. [53] considered a full state feedback controller and derived an AV controller based on optimal control to stabilize a ring road. Li et al. [19] further investigated the impact of the penetration rates and distributions of the optimal control method, in which optimal distributions based on \mathcal{H}_2 norm are shown to be dependent on penetration rates and the setup of CFMs. Although many controllers have successfully demonstrated the capabilities of improving traffic flows on the ring road in the literature, most of them are not generally benchmarked under different penetration rates and distributions. Since the penetration rates and distribution may have great impact on the traffic [19, 51], it is essential to evaluate controllers thoroughly under different penetration rates and distributions. Given that the analysis may generally not be tractable for all controllers, analysis based on simulations is done in our work. This work aims to make general comparisons of these controllers under different penetration rates and distributions, particularly focusing on controllers that have been validated against ring road traffic in simulations or real-world experiments. Kreidieh et al. [18] found that controllers generated in closed network scenarios with otherwise similar densities and perturbing behaviors confirms that closed network policies are transferable to open network scenarios. In their work on leading cruise control, Wang et al. [43] were able to verify the potential to control traffic using connected AVs on an open road.

Contribution. In this article, we assess the improvement of mixed autonomy traffic with AVs on a ring road under different penetration rates and distributions while all AV algorithms remain unchanged under different penetration rates and distributions. The time to stabilize, maximum headway, **vehicle miles traveled (VMT)**, and fuel economy are used to evaluate their performance. From the simulation experiments, we find that traffic condition improvement is generally independent of distribution of AVs, particularly when no cooperation among them is considered, except for two of the AV controllers considered in this work. The traffic condition is generally

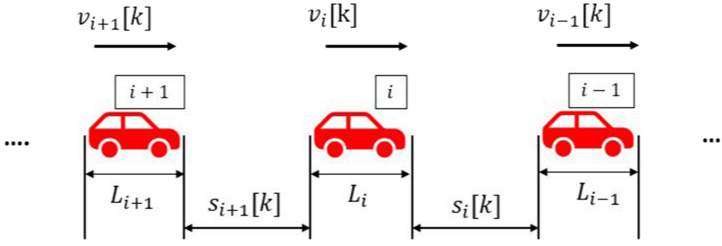


Fig. 1. CFM notation representation. The image shows three cars that are spaced, which acts as a headway with corresponding speed traveling in the same direction. The first car is $i - 1$, followed by the subject vehicle i and the vehicle behind the subject vehicle represented as $i + 1$.

improved with a higher penetration rate, but one of the AV algorithms shows a contrary trend. We show that the VMT and fuel economy are also improved with more AVs because of smoother traffic flow, except for one AV controller that shows reduced fuel economy even with improved traffic flow. Finally, among all AV algorithms in this study, the RL controller shows the most consistent improvement under all distributions and penetration rates.

The rest of the article is organized as follows. Section 2 details the notations and preliminaries in Section 2.1, followed by the detailed mathematical CFMs as HVs in Section 2.2 and various mathematical models of car-following controllers as AVs in Section 2.3. In Section 3, we study the performance of AVs by carrying out experiments on a ring road using a state-of-the-art traffic simulation platform considering various penetration rates and distribution of AVs for each AV model. Time to stabilize, maximum headway, VMT, and fuel economy are used to evaluate their performance. Section 4 concludes the article.

2 MATHEMATICS

This section is divided into three subsections. Section 2.1 defines the notations and preliminaries, whereas Section 2.2 deals with typical human behavior CFMs and Section 2.3 is dedicated to controllers designed for AVs.

2.1 Notations and Preliminaries

In this article, vehicle CFMs are discussed. Subscripts of variables indicate to which vehicle the variables are related. Vehicles are generally labeled with a number, increasing sequentially against traffic flow. Vehicles in the downstream are numbered with smaller numbers, and vehicles upstream are numbered with larger numbers. In a platoon of N vehicles, the vehicle indexed 1 is the leading vehicle in the platoon, and the last vehicle is indexed N . An illustration of the platoon is shown in Figure 1. The image shows three cars in a platoon that are traveling in the same direction. For convenience, a few commonly used variables are listed next:

- $x_i : [0, \infty) \rightarrow \mathbb{R}$: Rear end position of vehicle i
- $v_i : [0, \infty) \rightarrow \mathbb{R}$: Speed of vehicle i
- $a_i : [0, \infty) \rightarrow \mathbb{R}$: Acceleration of vehicle i
- $L_i \in \mathbb{R}$: Length of vehicle i
- $s_i : [0, \infty) \rightarrow \mathbb{R}$: Space headway between vehicle i and vehicle $i - 1$, which is equivalent to $x_{i-1} - x_i - L_i$
- $v_{\text{rel},i} : [0, \infty) \rightarrow \mathbb{R}$: Relative speed between the leading vehicle and the subject vehicle i ; $v_{\text{rel},i} := v_{i-1} - v_i$.

Table 1. Acronyms and Abbreviations

AVs	Automated vehicles	ACC	Adaptive cruise control
HVs	Human-driven vehicles	LACC	Linear adaptive cruise control
CFM	Car-following model	MLYAU1	Modified Lyapunov 1 controller
RL	Reinforcement learning	MLYAU2	Modified Lyapunov 2 controller
IDM	Intelligent driver model	LinOpt	Linear optimal controller
VMT	Vehicle miles traveled	MLP	Multilayer perceptron
AUG	Augmented Optimal Velocity Follow-the-Leader	GRU	Gated recurrent unit
BCM	Bilateral control model	PPO	Proximal policy optimization
FS	FollowerStopper controller	SUMO	Simulation of Urban Mobility
PI	Proportional-integral with saturation controller	ICs	Initial conditions
HBEFA	Handbook Emission for Road Transportation	FUZ	Fuzzy controller

Discrete models are considered in this article. Discrete dynamics of the vehicle motion are

$$x_i[k+1] = x_i[k] + v_i[k]\Delta t, \quad (1)$$

$$v_i[k+1] = v_i[k] + a_i[k]\Delta t, \quad (2)$$

where $\Delta t \in \mathbb{R}$ is the discretization step size. Acceleration of the vehicle will be determined based on CFMs and AV algorithms described in the following sections.

A list of abbreviations and acronyms used in this article is summarized in Table 1.

2.2 Intelligent Driving Model IDM as a Human Driver CFM

As mentioned in Section 1, there are many extensive studies to model how people drive on the road. The conceptual bases of these models are supported by empirical data [4]. Despite the numerous models developed, this is still an active field of research given the modeling challenges caused by heterogeneity of traffic and varying characteristics of drivers. Other examples of CFMs include the optimal velocity model [2, 3] second-order linear model [28], and IDM [39, 40]. Among these models, IDM is recognized for being capable of accurately representing realistic driver behavior [39]. Hence, IDM is adopted in this work and used to represent human-driven cars.

The work of Treiber et al. [39] and Treiber and Kesting [40] provided a comprehensive and instructive coverage of vehicular traffic flow dynamics and modeling in their work leading to the formulation of IDM, a CFM for the simulation of freeway and urban traffic. It describes the dynamics of the positions and velocities of single vehicles. The acceleration of IDM is shown next:

$$a_i[k] = a_{\max} \left[1 - \left(\frac{v_i[k]}{v_0} \right)^\delta - \left(\frac{s^*(v_i[k], v_{\text{rel},i}[k])}{s_i[k]} \right)^2 \right], \quad (3)$$

where $v_0 \in \mathbb{R}$ is the desired velocity, $a_{\max} \in \mathbb{R}$ is the maximum acceleration, $\delta \in \mathbb{R}$ is the acceleration exponent, $b \in \mathbb{R}$ is the desired deceleration, and $s^* : \mathbb{R} \times \mathbb{R} \rightarrow \mathbb{R}$ is the desired headway of the vehicle for a given vehicle speed and a relative speed, denoted by

$$s^*(v_i[k], v_{\text{rel},i}[k]) = s_0 + \max \left(0, v_i[k]T - \frac{v_i[k]v_{\text{rel},i}[k]}{2\sqrt{a_{\max}b}} \right), \quad (4)$$

where $T \in \mathbb{R}$ is the safe time headway and $s_0 \in \mathbb{R}$ is the jam distance or minimum gap. The parameters used in IDM are presented in Section 3.2. To replicate stop-and-go waves with IDM, the selection of the parameters are picked such that the criterion for ring road stability is not satisfied.

2.3 AV CFMs

This section discusses the known models that include controllers mainly developed for AVs, starting from level 1 (driving assistance capabilities) to having algorithms that may apply up to level 5 (fully) AVs. Note that as the level of autonomy increases, there are also increased capabilities with respect to what the vehicles on its own like the ones described for level 1 and level 2 here. Unlike human behavior CFMs, models introduced here are not meant to replicate human driving behavior. These AV CFMs were designed and meant to have better properties, e.g., stability, safety, efficiency, etc.

2.3.1 Augmented OV-FTL Model. Cui et al. [6] augmented the OV-FTL (optimal-velocity-follow-the-leader) model with a term penalizing the difference between the AV speed and the equilibrium speed $v_{eq} \in \mathbb{R}$:

$$a[k] = k_a(V(s_i[k]) - v_i[k]) + k_b \frac{v_{i-1}[k] - v_i[k]}{s_i[k]^2} + k_c(v_{eq} - v_i[k]), \quad (5)$$

where $k_a \in \mathbb{R}$, $k_b \in \mathbb{R}$, and $k_c \in \mathbb{R}$ are positive parameters; $V(\cdot) : \mathbb{R} \rightarrow \mathbb{R}$ is a monotonically non-decreasing function:

$$V(s_n) = \begin{cases} 0, & \text{if } s_n \leq s_{st}, \\ \frac{v_{max}}{2} \left(1 - \cos \left(\pi \frac{s_n - s_{st}}{s_{go} - s_{st}} \right) \right), & \text{if } s_{st} < s_n < s_{go}, \\ v_{max}, & \text{if } s_n \geq s_{go}, \end{cases} \quad (6)$$

where $s_{st} \in \mathbb{R}$, $s_{go} \in \mathbb{R}$ are parameters.

2.3.2 Bilateral Control Model. The **bilateral control model (BCM)** is a controller that is almost similar to **linear adaptive cruise control (LACC)**, except that instead of considering the relative speed and the spacing headway only with respect to the preceding vehicle as applied in LACC, it is now considering relative speeds and the spacing headways with respect to its preceding vehicle and its following vehicle wherein it is assumed that this information can be obtained by the subject vehicle using sensors in the front and in the back. By that, the vehicle tries to be halfway between the leading and the following vehicle. Following this, the i -th vehicle uses the following acceleration equation [15]:

$$a[k] = k_d (s_i[k] - s_{i+1}[k]) + k_v \left((v_{i-1}[k] - v_i[k]) - (v_i[k] - v_{i+1}[k]) \right) + k_p (v_{des} - v_i[k]), \quad (7)$$

where $k_d \in \mathbb{R}$, $k_v \in \mathbb{R}$, and $k_p \in \mathbb{R}$ are parameters that with any arbitrary positive constants will always lead to ring stability [16, 45]; $v_{des} \in \mathbb{R}$ is a design parameter representing the desired speed.

2.3.3 FollowerStopper. The **FollowerStopper controller (FS)** [34] generates the speed command $v_i^{cmd}(\cdot, \cdot) : \mathbb{R} \times \mathbb{R} \rightarrow \mathbb{R}$ based on the combinative conditions of the headway $s_i[k]$ and the relative speed $v_{rel,i}[k]$. The condition of the headway and the relative speed are divided into four regions. In each region, the safety speed command is determined to prevent the AV from crashing into the vehicle in front of it. Speed command v_i^{cmd} in each region is shown next, followed by the definition of each region:

$$v_i^{cmd}(s_i[k], v_{rel,i}[k]) = \begin{cases} 0 & \text{if } s_i[k] \leq \Delta x_1 \text{ (Stopping region)} \\ \hat{v}[k] \frac{s_i[k] - \Delta x_1}{\Delta x_2 - \Delta x_1} & \text{if } \Delta x_1 < s_i[k] \leq \Delta x_2 \text{ (Adaptation region I)} \\ \hat{v}[k] + (U - \hat{v}[k]) \frac{s_i[k] - \Delta x_2}{\Delta x_3 - \Delta x_2} & \text{if } \Delta x_2 < s_i[k] \leq \Delta x_3 \text{ (Adaptation region II)} \\ U & \text{if } \Delta x_3 < s_i[k] \text{ (Safe region)} \end{cases}, \quad (8)$$

where $\hat{v}[k] = \min\{\max\{v_{i-1}[k], 0\}, U\}$. A safe cruise speed $U \in \mathbb{R}$ is assigned as the reference speed in the safe region. In the stopping region, zero velocity is commanded. In the adaptation region (two parts), some average of desired and lead vehicle velocity is commanded. The boundary of each region is defined as follows:

$$\Delta x_j[k] = \Delta x_j^0 + \frac{1}{2d_j} (\Delta v_-[k])^2, \quad \forall j = 1, 2, 3, \quad (9)$$

where $\Delta v_-[k] = \min\{v_{\text{rel},i}[k], 0\}$. $\Delta x_1^0 \in \mathbb{R}$, $\Delta x_2^0 \in \mathbb{R}$, $\Delta x_3^0 \in \mathbb{R}$, $d_1 \in \mathbb{R}$, $d_2 \in \mathbb{R}$, and $d_3 \in \mathbb{R}$ are design parameters. Given the command speed, corresponding acceleration of the vehicle is

$$a_i[k] = \frac{v_i^{\text{cmd}}[k] - v_i[k]}{\Delta t}.$$

2.3.4 Proportional-Integral with Saturation. The **proportional-integral with saturation controller (PI)** is a controller for speed control. It has been implemented on the real vehicle and used to dissipate stop-and-go waves in the circuit ring road [8, 34]. The controller is modeled in the discrete manner, and $v^{\text{cmd}}[k]$ denotes the speed command at timestep $k \in \mathbb{Z}_{\geq 0}$:

$$v^{\text{cmd}}[k+1] = \beta[k] \left(\alpha[k] v^{\text{target}}[k] + (1 - \alpha[k]) v^{\text{lead}}[k] \right) + (1 - \beta[k]) v^{\text{cmd}}[k]. \quad (10)$$

The speed command $v^{\text{cmd}}[k] \in \mathbb{R}$ is basically the low-pass filtered output of the weighted average of the preceding vehicle speed $v^{\text{lead}}[k] \in \mathbb{R}$ and the subject vehicle's own target speed $v^{\text{target}}[k] \in \mathbb{R}$. The AV's target speed is defined as follows:

$$v^{\text{target}}[k] = \bar{U}[k] + v^{\text{catch}} \times \min \left\{ \max \left\{ \frac{s_i[k] - g_l}{g_u - g_l}, 0 \right\}, 1 \right\}, \quad (11)$$

where $\bar{U}[k] \in \mathbb{R}$ is the temporal average of own speed over an historic interval, which is $\bar{U}[k] = \frac{1}{m} \sum_{j=k-1}^{k-m} v^{\text{AV}}[j]$; $v^{\text{catch}} \in \mathbb{R}$, $g_l \in \mathbb{R}$, and $g_u \in \mathbb{R}$ are design parameters. $v^{\text{catch}} \in \mathbb{R}$ is the catch-up speed that allows the target speed to be larger than average speed in the past so that the AV can speed up when the headway is large. The parameters $\alpha[k] \in \mathbb{R}$ and $\beta[k] \in \mathbb{R}$ are formulated to be dependent on the headway $s_i[k] \in \mathbb{R}$ at timestep k , which are shown as follows:

$$\alpha[k] = \min \left\{ \max \left\{ \frac{s_i[k] - \Delta x^s[k]}{\gamma}, 0 \right\}, 1 \right\}, \quad (12)$$

$$\beta[k] = 1 - \frac{1}{2} \alpha[k], \quad (13)$$

where $\gamma \in \mathbb{R}$ is a design parameter and $\Delta x^s[k] \in \mathbb{R}$ is defined as

$$\Delta x^s[k] = \max \left\{ 2 \left(v^{\text{lead}}[k] - v^{\text{AV}}[k] \right), 4 \right\}. \quad (14)$$

This controller has also been called the *MLB controller* in the work of Delle Monache et al. [8]. Given the speed command, the corresponding acceleration command is

$$a_i[k] = \frac{v_i^{\text{cmd}}[k] - v_i[k]}{\Delta t}.$$

2.3.5 Linear Adaptive Cruise Control. **Adaptive cruise control (ACC)** is a driver-assistance system that can automatically adjust the vehicle's speed to maintain safe spacing from the preceding vehicle, which is commonly seen on many production vehicles. Linear models can be used to

approximate the dynamics of the ACC system [5, 20, 22, 25, 31, 52]. In this work, we study the performance of ACC using approximation of a first-order ordinary differential equation. The model described in the work of Rajamani [30] is adapted in this work:

$$a_i[k+1] = \left(1 - \frac{\Delta t}{\tau}\right) a_i[k] + \frac{\Delta t}{\tau} a_{\text{cmd},i}[k], \quad (15)$$

$$a_{\text{cmd},i}[k] = k_1 e_{x,i}[k] + k_2 v_{\text{rel},i}[k], \quad (16)$$

$$e_{x,i}[k] = s_i[k] - h v_i[k], \quad (17)$$

where $a_{\text{cmd},i}[k] \in \mathbb{R}$ is the command acceleration of the vehicle, $e_{x,i}[k] \in \mathbb{R}$ is the gap error, $\tau \in \mathbb{R}$ is the lag time of the system, h is the desired time gap, and $k_1 \in \mathbb{R}$ and $k_2 \in \mathbb{R}$ are positive design parameters. These parameters can be calibrated using the collected data from the field experiment.

2.3.6 Optimal Control Strategy. Zheng et al. [53] proposed a strategy of optimal control. The human driver CFM is first linearized. Suppose that vehicle 1 is the AV; linear optimal control is derived in the following form:

$$a_i[k] = - \left[k_{1,1}(s_i[k] - s_c^*) + k_{1,2}(v_i[k] - v^*) + \sum_{j=2}^N k_{j,1}(s_{i+j-1}[k] - s^*) + k_{j,2}(v_{i+j-1}[k] - v^*) \right]. \quad (18)$$

On a ring road, where vehicle 1 is following vehicle N , the index of the vehicle is cyclic (i.e., $s_i = s_{i+N}$, $v_i = v_{i+N}$). Parameters $k_{j,1} \in \mathbb{R}$, $k_{j,2} \in \mathbb{R}$, $\forall j \in \{1, \dots, N\}$ are obtained by optimal control. $s_c^* \in \mathbb{R}$ is the average following distance of every vehicle on the ring road. To obtain these parameters, we define $K = [k_{1,1}, k_{1,2}, k_{2,1}, k_{2,2}, \dots, k_{N,1}, k_{N,2}] \in \mathbb{R}^{1 \times 2N}$ and let K equal ZX^{-1} , where $Z \in \mathbb{R}^{1 \times 2N}$ and $X \in \mathbb{R}^{2N \times 2N}$ are the optimizer of the following optimization problem:

$$\begin{aligned} & \min_{X, Y, Z} \text{Trace}(QX) + \text{Trace}(RY) \\ & \text{subject to } (AX - BZ) + (AX - BZ)^T + HH^T \leq 0, \\ & \begin{bmatrix} Y & Z \\ Z^T & X \end{bmatrix} \geq 0, X \geq 0, \end{aligned}$$

where $A \in \mathbb{R}^{2N \times 2N}$, $B \in \mathbb{R}^{2N}$, and $H \in \mathbb{R}^{2N}$ are matrices for the state space model of the linearized ring road dynamics. Q and R are design parameters, which are defined as $Q = \text{diag}(\gamma_s^2, \gamma_v^2, \dots, \gamma_s^2, \gamma_v^2) \in \mathbb{R}^{2N \times 2N}$ and $R = \gamma_u^2 \in \mathbb{R}$. Although the optimal control can be redesigned to achieve optimal performance under different penetration rates and different distributions [19], in this work, for our purpose, we do not redesign the controller for different penetration rates and distributions. The optimal controller described in this section is derived based of traffic of one AV and 22 HVs and tested under all scenarios in the simulation studies.

2.3.7 Lyapunov-Based Controller. Delle Monache et al. [8] proposed two types of Lyapunov-based controller. The controllers are first derived using Lyapunov-like function. Controllers are then discretized considering that the controllers are deployed on the digital system, where the target speed at each timestep is issued as the input to the lower system of the AV. The first Lyapunov-based controller is as follows:

$$v_i^{\text{target},1}[k+1] = (u[k] - \bar{v}[k]) \exp(-\Delta t) + \bar{v}[k]. \quad (19)$$

The second controller is as shown next:

$$v_i^{\text{target},2}[k+1] = \left(u[k] - \frac{v_{i-1}[k] + \bar{v}[k]}{2} \right) \exp(-\Delta t) + \frac{v_{i-1}[k] + \bar{v}[k]}{2}. \quad (20)$$

$v_i^{\text{target},1}[k+1] \in \mathbb{R}$, $v_i^{\text{target},2}[k+1] \in \mathbb{R}$ are target speeds of the i -th vehicle of the first and the second controller at timestep $k+1$. $u[k] \in \mathbb{R}$ and $\bar{v}[k] \in \mathbb{R}$ are defined as follows:

$$u[k+1] = \beta[k](\alpha[k]v_i^{\text{target},j}[k] + (1-\alpha[k])v_{i-1}[k]) + (1-\beta[k])u[k], \quad (j = 1, 2), \quad (21)$$

$$\bar{v}[k] = \min \left\{ \frac{\sum_{m=1}^{k-1} v_{i-1}[m]}{k-1}, \frac{\sum_{m=1}^{k-1} u[m]}{k-1} \right\}. \quad (22)$$

Controller gains $\alpha[k] \in \mathbb{R}$ and $\beta[k] \in \mathbb{R}$ are defined as follows:

$$\alpha[k] = \min \left\{ \max \left\{ \frac{s_i[k] - \Delta x^s[k]}{\gamma}, 0 \right\}, 1 \right\}, \quad (23)$$

$$\beta[k] = 1 - \frac{1}{2}\alpha[k], \quad (24)$$

where

$$\Delta x^s[k] = \max \{ 2(v_{i-1}[k] - v_i[k]), 4 \}.$$

Given the target speed, the corresponding acceleration command is

$$a_i[k] = \frac{v_i^{\text{target},j}[k] - v_i[k]}{\Delta t}.$$

2.3.8 Fuzzy Controller. Haulcy et al. [13] proposed a fuzzy controller for stabilizing a ring road. In the fuzzy logic, the space headway and the relative speed are processed to determine the desired speed change. Triangular shape membership functions are constructed to represent the levels of the different classes of the distances and the speed differences. The speed change command is determined following the inference process and the defuzzification process.

2.3.9 RL Control. RL is learning to do tasks wherein the agent (i.e., the learner) does some action without having to be told what action to do. The agent does random actions at first and maps out each of these actions to determine which among them maximizes the numerical rewards. Mathematically, an agent learns a policy $\pi(\text{state}) = \text{action}$, and maps from states *state* to actions *action*, to achieve a goal in an environment under uncertainty. Through repeated environment interactions, an RL agent strives to develop an optimal policy π^* , which maximizes the sum of the rewards. RL is often used in solving sequential decision-making problems [36]. To deal with the traffic control with the RL, Wu et al. [49, 50] proposed a framework for traffic control using deep RL. The framework integrates the traffic simulation environment called **Simulation of Urban Mobility (SUMO)** and the RL library, such as rllab [9] and rllib [21], so that the policy can be learned to optimize the cumulative reward using sampled data from SUMO. The policy usually consists of neural networks and may be of several forms. Two policies—the multilayer perceptron and the gated recurrent unit—are proposed for a ring road problem in the work of Wu et al. [50]. The multilayer perceptron is a classical (feedforward) artificial neural network with multiple hidden layers and utilizes back propagation to optimize its parameters. Gated recurrent units are recurrent neural networks capable of storing memory on the previous states of the system through the use of parameterized update and reset gates, which are also optimized by the policy gradient method. One of the advanced RL algorithms is Proximal Policy Optimization [33], which is said to perform comparably or better than state-of-the-art approaches. Other advanced RL, such as the soft-actor critic [12], not covered in this work, can also be investigated in the near future. The RL control tested in this work is trained on the ring road of one agent and 21 HVs. The *state* is the distance between the agent and its leading vehicle ($s_i[k]$), the leading vehicle speed ($v_{i-1}[k]$), and the agent speed ($v_i[k]$). The *action* is the agent acceleration ($a_i[k]$). Suppose that the RL agent is

Table 2. Summary of the AV Models on a Ring Road

AV Model	Input	Controller Type	Design Parameters	Design Method
AUG	s_i, v_i, v_{i-1}	Linear	k_a, k_b, k_c, v_{eq}	Model based
BCM	$s_i, s_{i+1}, v_i, v_{i-1}, v_{i+1}$	Linear	k_d, k_v, k_p, v_{des}	Model based
FS	s_i, v_i, v_{i-1}	Nonlinear	$U, \Delta x_1^0, \Delta x_2^0, \Delta x_3^0, d_1, d_2, d_3$	Heuristic
PI	s_i, v_i, v_{i-1}	Nonlinear	$v^{catch}, g_u, g_l, \gamma$	Heuristic
LACC	s_i, v_i, v_{i-1}	Linear	k_1, k_2, h	Model based
LinOpt	$s_i, v_i, \forall i \in \{1, 2, \dots, N\}$	Linear	$\gamma_s, \gamma_v, \gamma_u$	Model based
MLYAU1	v_i, v_{i-1}	Linear	γ	Model based
MLYAU2	v_i, v_{i-1}	Linear	γ	Model based
FUZ	s_i, v_i, v_{i-1}	Nonlinear	See details in the work of Haulcy et al. [13]	Heuristic
RL	s_i, v_i, v_{i-1}	Nonlinear	See details in the work of Wu et al. [48]	Learning based

the i -th vehicle in the ring road; the reward $r_i[k] \in \mathbb{R}$ is designed in a way that high average speed of all vehicles is rewarded, whereas high acceleration of the agent is penalized. The reward at each timestep is

$$r_i[k] = \eta_1 \sum_{j=1}^{22} v_j[k] - \eta_2 \max\{0, a_i[k]\}.$$

Once the policy is trained on the ring road of one agent and 21 HVs, it is tested under different penetration rates and distributions with no modification.

2.3.10 Summary Table for AV Controllers. In Table 2, properties of the AV models considered in this article are summarized, including the needed input, the controller type, the design parameters, and the design method. In terms of input needed for the controllers, all the controllers need at least the speed measurements of the leading vehicle and the subject vehicle, and most of them also use the measurement of the spacing ahead of the subject vehicle, except MLYAU1 and MLYAU2. Without using the feedback of the spacing ahead, the following distance of MLYAU1 and MLYAU2 cannot be controlled. In addition to the spacing ahead and the speed of the leading vehicle, the BCM also uses the spacing behind and the speed of the following vehicle. The optimal control needs the most information, not only the spacing and the speeds of the vehicles nearby but also spacing and speeds of all vehicles on the ring road. To access this information, wireless communication may be needed between vehicles. The third column of Table 2 shows the types of the controller. Four of the controllers are nonlinear controllers, and the rest of the controllers are linear. The design parameters of the controllers are listed in the fourth column, except FUZ and RL, because there are too many parameters of these two controllers to show here. The references for these two controllers are provided instead. Inspired by the classification in the work of Wang et al. [44], the last column summarizes the ways controllers are derived. Three controllers are designed based on observations in the real world. RL is the only controller that is based on learning. The rest of the controllers are based on analyses of the CFMs.

3 SIMULATION

3.1 Simulation Platform

SUMO [23] is mainly used to simulate traffic flow in a ring road. We used this simulation software since it is open source, enabling interested parties to reproduce the results we have. SUMO has the capability to generate microscopic models of inter-modal traffic systems including road vehicles, public transport, and pedestrians. It allows customized models and has various APIs to control the simulations remotely. It also allowed us to calculate the fuel economy, based on the Handbook Emission Factors for Road Transport 3 Euro 4 passenger car emission model.

To run the simulations in SUMO, we also utilized existing libraries of code available in Flow [47, 48] which is a computational framework mainly developed to enable the use of RL methods such as policy gradient methods for traffic control and enables benchmarking of the performance of classical controllers, which is then built to work on the SUMO microsimulator. Flow is developed by the Mobile Sensing Lab at the University of California, Berkeley.

This study is the general investigation of behavior of vehicles driving on a closed-circuit road. Since the ring itself is a closed loop, we used a continuous router that ensures the continuous rerouting of the vehicles in a closed loop. This class is useful if vehicles are expected to continuously follow the same route, and the said route is repeated once it reaches its end.

3.2 Simulation Setup and Simulation Parameters

We are interested in the dynamic behavior of the closed-circuit ring road. The simulation environment is set up similar to the real experiment shown in the work of Stern et al. [34]. There are 22 vehicles on the single-lane-circuit ring road, which has a radius of 41.38 m (circumference is 260m). At the beginning of the simulation, the vehicles are placed uniformly, with each headway being the same, and the initial speeds are all zero. Depending on the scenarios (Section 3.3) running, each vehicle is assigned as an HV or as a different type of AV. In each simulation run, there is always a 300-second warm-up, in which all vehicles are running with IDM to make the ring traffic in the status of having stop-and-go waves. After that, the assigned AVs switch to the automated control. For each model, values of parameters used in the simulations in this work are summarized in this section. Selection of parameters may have an influence on the performance. For the purpose of benchmarking, values of the original articles are used if they are available. Otherwise, values based on design criteria shown in the origin articles are used. None of these values are fine-tuned, although performance may be improved after careful tuning:

- *Intelligent driver model (IDM)*: The parameters chosen for IDM are as follows: acceleration component $\delta = 4$, safe time headway $T = 1$, maximum acceleration $a_{\max} = 1$, desired deceleration $b = 1.5$, jam distance $s_0 = 2$, and maximum speed $v_0 = 30$ [40, Chapter 11].
- *Augmented OV-FTL (AUG)*: $k_a = 1$, $k_b = 1$, $k_c = 11.0$, $h_{st} = 2$, $h_{go} = 15$, $v_{\max} = 30$, and $v_{eq} = 4.8$, where k_a and k_b are arbitrary positive numbers, and k_c is selected based on the criterion shown in the work of Cui et al. [6]; h_{st} , h_{go} , and v_{\max} are default values in Flow [48]; v_{eq} is the equilibrium speed of 22 IDMs on the ring road.
- *Bilateral control model (BCM)*: The bilateral CFM (Section 2.3.2) and the parameters of the controller used are $k_d = 1$, $k_v = 1$, $k_p = 1$, $v_{des} = 4.8$. It has been proven in the work of Wang and Horn [45] that the system of BCM vehicles is chain stable for arbitrary values of k_d and k_v that are greater than zero. v_{des} is picked as the equilibrium speed of 22 IDMs on the ring road.
- *FollowerStopper (FS)*: The parameters defining the four regions of the controller are as follows: $\Delta x_1^0 = 4.5$, $\Delta x_2^0 = 5.0$, and $\Delta x_3^0 = 6.0$. In addition, the deceleration rates are defined to be $d_1 = 1.5$, $d_2 = 1.0$, $d_3 = 0.5$, and $U = 4.8$. Parameters shown in the work of Stern et al. [34] are used. U is the target speed of the FollowerStopper. It is picked as the equilibrium speed of 22 IDMs on the ring road.
- *Proportional-Integral with saturation (PI)*: Parameters used in simulation are $\gamma = 2$, $g_1 = 7$, $g_u = 30$, and $v^{catch} = 1$. Parameters shown in the work of Stern et al. [34] are used.
- *Linear Adaptive Cruise Control (LACC)*: All the ACC-controlled vehicles have the same parameters for dynamics and control: $\tau = 0.1$, $h = 1.4s$, $k_1 = 0.4$, and $k_2 = 0.7$. These parameters are picked such that its equilibrium speed is close to that of IDM, and string stability condition for a linear CFM can be satisfied.

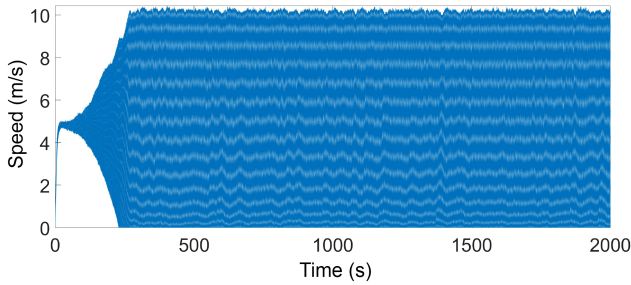


Fig. 2. Speed profiles of all IDM vehicles on the ring. The stop-and-go waves are fully developed at around 300 seconds and persist for the rest of the time.

- *Linear optimal controller (LinOpt)*: The controller gains are designed using the gains as follows: $\gamma_s = 1$, $\gamma_v = 1$, $\gamma_u = 1$. These values are not specified in the original work and are arbitrarily selected here.
- *Lyapunov-based controllers (MLYAU1 and MLYAU2)*: For both type 1 and type 2, they have the same parameter: $\gamma = 2$. The parameter value shown in the work of Delle Monache et al. [8] is used.

3.3 Scenario

Given the goal of this article, we designed our simulations to include cases of both mixed-autonomy traffic with varying percentages of AVs in the system, and also the case where we have full autonomy.

Baseline case (no automation). In this article, the baseline scenario we are considering is all HVs on the ring. We are using IDM to model the human driving behavior. To stimulate instability of the ring road model to reproduce stop-and-go waves, acceleration noises are intentionally injected to all CFMs. Another way of stimulating speed fluctuations is by inducing sudden speed changes of vehicles in the traffic (e.g., [11, 15, 53]). In this work, persistent excitation of the traffic with acceleration noises are used, because we can produce stop-and-go waves more easily by doing this. Speed profiles of the 22 vehicles of IDM on the ring are shown in Figure 2. The plot shows how the speed profiles of the vehicles greatly vary with time especially after a certain time greater than 200 seconds.

Mixed autonomy traffic (varying percentages of AV penetration). As an integral part of the simulations, we included a variation in the number of AVs in the system to test how the autonomous controllers perform in a mixed-autonomy condition to see if there is also significance in their performance depending on the percentage of penetration. Besides the penetration rate, we also investigate the impact of different distributions of AVs among HVs. Table 3 summarizes the setups for scenarios we are studying in this article. In *scenario I: platooned*, AVs are placed in the clustered manner, of which AVs are placed consecutively and HVs are also placed consecutively. Penetration of 1 AV all the way to 22 AVs is studied. Then, *scenario II: evenly distributed* is the case where the AVs are placed as evenly distributed as possible. That is when the minimum number of HVs between any two AVs is maximized. In this scenario, a maximum of 11 AVs are placed on the ring and studied, because any number more than 11 will no longer keep AVs separated evenly by HVs. Simulation results of these scenarios are shown in the next section. To help the reader visualize scenarios, Tables 4 and 5 are provided, showing the types of each vehicle on the road under different penetration rates in different scenarios. To compare the performance of controllers

Table 3. Scenarios of Experiments in Flow

	Scenario I	Scenario II
AV(s) Activation Time	300	300
ICs (Positions)	$s_i[0] = s_{eq} + \tilde{s}_i, \forall i = \{1, \dots, 22\}$	$s_i[0] = s_{eq} + \tilde{s}_i, \forall i = \{1, \dots, 22\}$
ICs (Speeds)	$v_i[0] = 0, \forall i = \{1, \dots, 22\}$	$v_i[0] = 0, \forall i = \{1, \dots, 22\}$
AV Distribution	Clustered	Evenly distributed
Number of AVs (= n)	$n \in \{1, 2, \dots, 22\}$	$n \in \{2, \dots, 11\}$
IDM Noise	0.1	0.1

$s_{eq} := (2\pi R_{ring} - \sum_{i=1}^{22} L_i)/22$, where $R_{ring} \in \mathbb{R}$ is radius of the ring road, and $\tilde{s}_i \in \mathbb{R}$ are random variables and are sampled such that $\sum_{i=1}^{22} \tilde{s}_i = 0$ to keep the sum of the headway matching the perimeter of the ring road. AV(s) Activation Time is the time at which AV controllers start to actively control the vehicles. ICs (Positions) are the initial conditions of vehicle positions on the ring road. ICs (Speeds) are the initial conditions of vehicle speeds on the ring road. AV Distribution is the way AVs are distributed among other vehicles. Number of AVs is the number of AVs being placed on the ring road. IDM Noise is the magnitude of the acceleration noise (in $m s^{-2}$) added to vehicles. The distributions of AVs for scenario I are shown in Table 4, and the distributions of AVs for scenario II are shown in Table 5.

Table 4. AV Distribution for Scenario I: Platooned Under Different Penetration Rates

(%)	Vehicle Type																			
4.55	AV	HV																		
9.09	AV	AV	HV																	
13.64	AV	AV	AV	HV																
18.18	AV	AV	AV	AV	HV															
22.73	AV	AV	AV	AV	AV	HV														
27.27	AV	AV	AV	AV	AV	AV	HV													
31.82	AV	AV	AV	AV	AV	AV	AV	HV												
36.36	AV	AV	AV	AV	AV	AV	AV	AV	HV											
40.91	AV	AV	AV	AV	AV	AV	AV	AV	AV	HV										
45.45	AV	AV	AV	AV	AV	AV	AV	AV	AV	AV	HV									
50.00	AV	AV	AV	AV	AV	AV	AV	AV	AV	AV	AV	HV								
54.55	AV	AV	AV	AV	AV	AV	AV	AV	AV	AV	AV	AV	HV							
59.09	AV	AV	AV	AV	AV	AV	AV	AV	AV	AV	AV	AV	AV	HV						
63.64	AV	AV	AV	AV	AV	AV	AV	AV	AV	AV	AV	AV	AV	AV	HV	HV	HV	HV	HV	HV
68.38	AV	AV	AV	AV	AV	AV	AV	AV	AV	AV	AV	AV	AV	AV	AV	HV	HV	HV	HV	HV
72.73	AV	AV	AV	AV	AV	AV	AV	AV	AV	AV	AV	AV	AV	AV	AV	AV	HV	HV	HV	HV
77.27	AV	AV	AV	AV	AV	AV	AV	AV	AV	AV	AV	AV	AV	AV	AV	AV	AV	HV	HV	HV
81.82	AV	AV	AV	AV	AV	AV	AV	AV	AV	AV	AV	AV	AV	AV	AV	AV	AV	AV	HV	HV
86.36	AV	AV	AV	AV	AV	AV	AV	AV	AV	AV	AV	AV	AV	AV	AV	AV	AV	AV	AV	HV
90.91	AV	AV	AV	AV	AV	AV	AV	AV	AV	AV	AV	AV	AV	AV	AV	AV	AV	AV	AV	HV
95.45	AV	AV	AV	AV	AV	AV	AV	AV	AV	AV	AV	AV	AV	AV	AV	AV	AV	AV	AV	AV
100.00	AV	AV	AV	AV	AV	AV	AV	AV	AV	AV	AV	AV	AV	AV	AV	AV	AV	AV	AV	AV

in terms of capabilities of dissipating stop-and-go waves, the controllers would only be activated after 300 seconds, a time at which the stop-and-go waves are fully formed.

3.4 Results

Some simulation results are shown in this section, and performance of the AV algorithms is evaluated. The metrics we are using for evaluation include time to stabilize, maximum final gap, VMT, and fuel economy.

Definition (Time to Stabilize). The time to stabilize is the minimum time it takes for the standard deviation of the speeds across all vehicles to become smaller than 0.1, which is the noise we intentionally inject into the acceleration command. To be more precise, the mathematical description

Table 5. AV Distribution for Scenario II: Evenly Distributed Under Different Penetration Rates

%	Vehicle Type																			
	AV	HV	AV	HV																
9.09	AV	HV	AV	HV																
13.64	AV	HV	HV	HV	HV	HV	AV	HV	AV	HV	HV	HV	HV	HV						
18.18	AV	HV	HV	HV	HV	AV	HV	HV	HV	HV	HV	AV	HV	HV	HV	HV	AV	HV	HV	HV
22.73	AV	HV	HV	HV	AV	HV	HV	HV	AV	HV	HV	HV	AV	HV	HV	HV	HV	AV	HV	HV
27.27	AV	HV	HV	HV	AV	HV	HV	AV	HV	HV	HV	AV	HV	HV	HV	AV	HV	HV	AV	HV
31.82	AV	HV	HV	AV	HV	HV	AV	HV	AV	HV	HV	AV	HV	HV	AV	HV	HV	HV	AV	HV
36.36	AV	HV	HV	AV	HV	AV	HV	AV	HV	AV	HV									
40.91	AV	HV	AV	HV	HV	AV	HV	AV	HV	HV	AV	HV	AV	HV	HV	AV	HV	AV	HV	AV
45.45	AV	HV	HV	AV	HV	HV	AV	HV	AV	HV	AV	HV								
50.00	AV	HV	AV	HV	AV	HV	AV	HV	AV	HV	AV	HV	AV	HV	AV	HV	AV	HV	AV	HV

is as follows:

$$T_{\text{stable}} = \arg \min_t \left\{ t : \sqrt{\frac{1}{21} \sum_{i=1}^{22} (v_i[k] - \mu[k])^2} \leq 0.1, \mu[k] = \sum_{i=1}^{22} v_i[k] \right\} - t_{\text{activation}}, \quad (25)$$

where $t_{\text{activation}}$ is the time when we switch on the AV, which is 300 seconds in our simulation. The shorter time implies better wave dissipation capability.

Definition (Maximum Final Gap). The maximum final gap is the maximum gap between any of two consecutive vehicles on the ring if a ring road is stable. This can be used to evaluate the efficiency of the use of spacing. Smaller is better. The formal mathematical definition is as follows:

$$\bar{s}_{\text{final}} = \max_{t \in [t_{\text{activation}} + T_{\text{stable}}, T_{\text{final}}]} \max_{\forall i=1,2,\dots,22} s_i[k], \quad (26)$$

where T_{final} is the timestep at the end of the simulation. To reduce the variations of these values because of randomness of the microsimulation, the values we are showing in the following are averages of 10 simulation runs. Because of the randomness, for a few of the controllers, some of the stable(unstable) results are not 100% reproducible. In other words, for a few AVs, under the same distribution and the same penetration rate, the simulations may not always be stable(unstable). For those marginal cases, we can say they are stable if more than 50% of the simulation runs are stable. For reference, we keep the number of unstable runs for each scenario and show them in Appendix A.

3.4.1 Scenario 1. Given the metrics defined, we can now evaluate the performance of different AV controllers. In the first scenario, the AV penetration rate from 0% to 100% is studied, where AVs are placed in the platoon. Some AV controllers can successfully stabilize the ring at a relative low penetration rate, whereas some need a higher penetration rate to stabilize the ring. Table 6 shows the minimum number of AVs needed to stabilize the ring and their corresponding time to stabilize, max gap, VMT, and fuel economy. To be noted, FUZ cannot stabilize the ring for any penetration rate. Therefore, no values are available. To illustrate the simulation, speed profiles of each vehicle of each case in the table are shown in Figure 3, and headways of each case in the table are shown in Figure 4, where red curves represent AVs and blue curves represent HVs. Results of FUZ are not shown here because the ring is not stabilized for any penetration rates. Table 6 also shows the VMT and the fuel economy for AVs that stabilized the traffic on the ring. The fuel economy is calculated using the built-in fuel consumption model of SUMO, which uses the HBEFA 3 Euro 4 passenger car emission model.

Based on Table 6, we can tell that the following controllers are able to stabilize the traffic on the ring with a minimum of one AV: FollowerStopper, PI, the linear optimal controller, Lyapunov-based controllers type 1 and type 2, and RL. Although AUG and BCM need four AVs and LACC needs nine AVs to stabilize the ring, the rest of the controllers need only one AV to stabilize the

Table 6. Average Performance Comparison of Scenario I

Controller	Minimum No. of AVs to Stabilize	Time to Stabilize (in seconds)	Max Gap (in meters)	VMT	Fuel economy (in miles per gallon)
AUG	4	88.29	12.19	118.23	16.21
BCM	4	319.68	12.11	128.59	21.46
FS	1	270.85	12.96	126.54	20.51
FUZ	Unstable	N/A	N/A	N/A	N/A
LACC	9	1,104.77	12.14	130.15	21.15
LinOpt	1	471.23	12.19	125.78	20.89
MLYAU1	1	62.64	116.49	21.83	7.39
MLYAU2	1	625.66	39.65	99.83	16.15
PI	1	263.74	12.03	125.67	20.71
RL	1	102.20	13.12	142.64	20.64

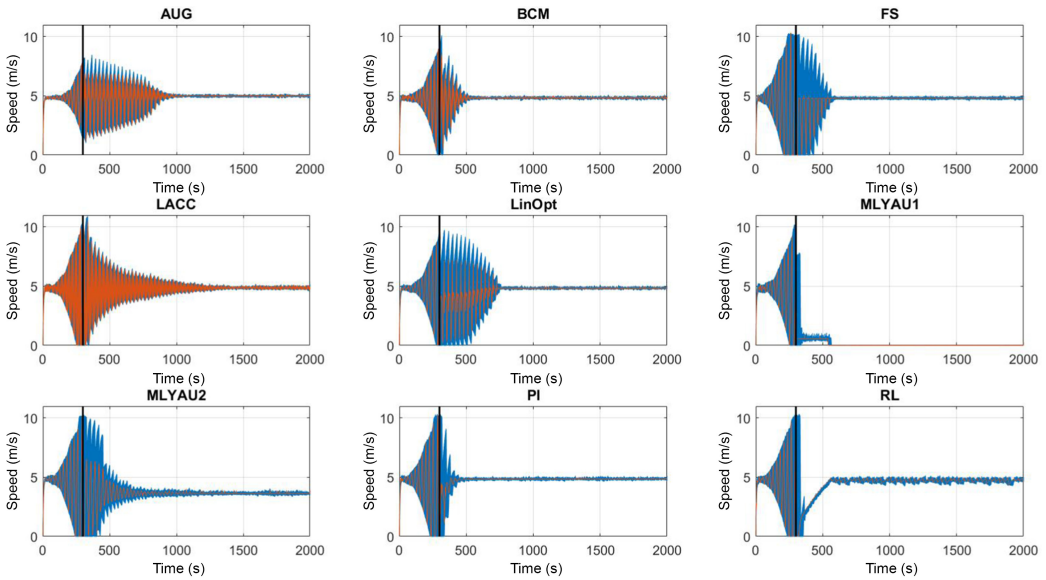


Fig. 3. Speed profiles of the stabilized results: red, AV; blue, HV; black, indication of the beginning of AV control. For the results of AUG and BCM, four AVs are placed on the ring road. For the result of LACC, nine AVs are placed on the ring road. For the result of the rest of the AVs, only one AV is placed on the ring road.

ring. Among these controllers, the Lyapunov-based controller type 1 (2.3.7) yields the fastest time to stabilize. However, from Figure 3, it is notable that after a few seconds in which the vehicles are stable, all of them simply stop. This is a trivial solution to be stable. Because of this, we can consider that the RL controller performs the best in terms of time to stabilize.

By looking at the headway, we can observe whether the traffic flow density on the ring road is uniform. We can observe that the headway between vehicles converges to a steady state when the traffic on the ring road is stable for all cases in Figure 4. Most AV controllers have similar headway, except MLYAU1 and MLYAU2, which have relative large headway. MLYAU1 gives the highest headway since the vehicles go to a complete stop a few seconds after being stable, creating a huge gap between the AV and the HVs. The baseline values of VMT and fuel economy are 96.71 miles and 13.43 miles per gallon when all vehicles are HVs. In terms of VMT, all cases in the table perform better than the baseline, because the flow is more smoother, except MLYAU1 basically

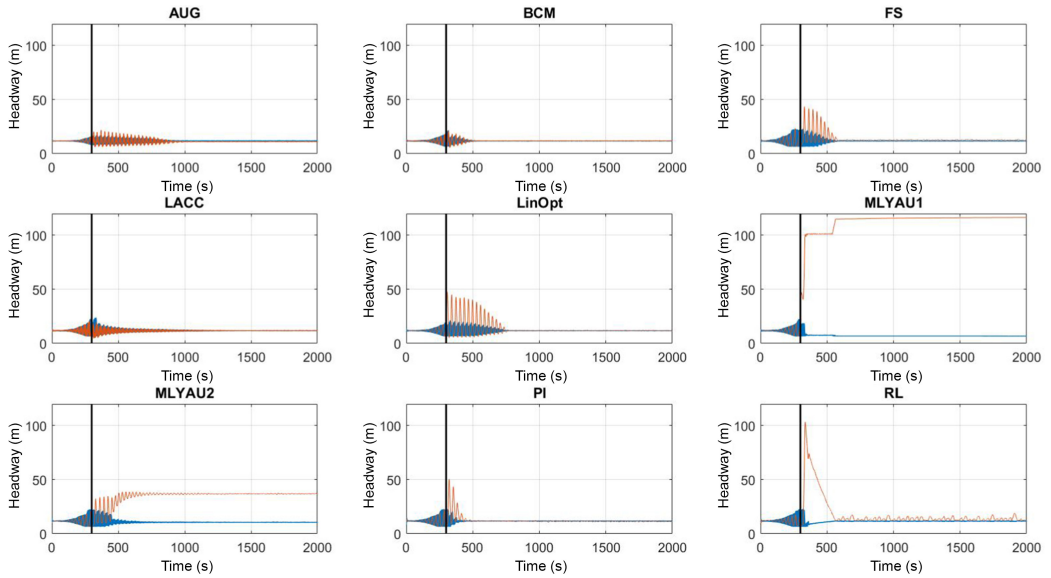


Fig. 4. Headway profiles of the stabilized results: red, AV; blue, HV; black, indication of the beginning of AV control. For the results of AUG and BCM, four AVs are placed on the ring road. For the result of LACC, nine AVs are placed on the ring road. For the result of the rest of the AVs, only one AV is placed on the ring road.

blocks the traffic, as mentioned. Fuel economy for all cases are generally better than the baseline as well, except MLYAU1.

Figure 5 further shows time to stabilize, maximum final gap, VMT, and fuel economy across different numbers of AVs on the ring. In Figure 5(a) and Figure 5(b), we neglect data points of unstable simulation results. In Figure 5(a), it can be observed that, generally, the time needed to be stable is shorter with more AVs on the ring, except PI. PI eventually makes the traffic turn into total chaos when there are more than eight AVs (~36% penetration rate) on the ring.

In Figure 5(b), we can also observe that the maximum headway is also not very dependent on the number of AVs on the ring, but it is relatively dependent on the AV types. It should be noted that MLYAU1 has relatively large headway because what it is doing is basically stopping all the traffic behind.

Figure 5(c) shows the comparison of VMT and Figure 5(d) shows the fuel economy. In terms of VMT, we can see that the AVs generally improve the VMT, except FUZ, which is not stable, and MLYAU1, which basically stops the traffic as we saw previously. The VMT is improved because the traffic flow is smoother than the baseline scenario. The VMT is generally positively related to the stability of the ring road. The VMT is almost the same for AVs whose stabilizing time is almost the same for different penetration rates. For AVs that get more stable (shorter stabilizing time) with an increasing penetration rate, the VMT is increasing with the penetration rates (e.g., BCM, LACC, AUG). However, for the AV that becomes less stable at higher penetration rates, the VMT decreases (e.g., PI). For fuel economy, we can observe that the fuel economy is improved for AVs with better stability. Whereas most AVs have generally improved fuel economy than the baseline case, except some AVs, both FUZ and MLYAU1 have worse fuel economy, because they either make the traffic less stable or block the traffic. Fuel economy generally gets better with increased penetration rates. This is particularly significant for the AVs that are not stable at lower

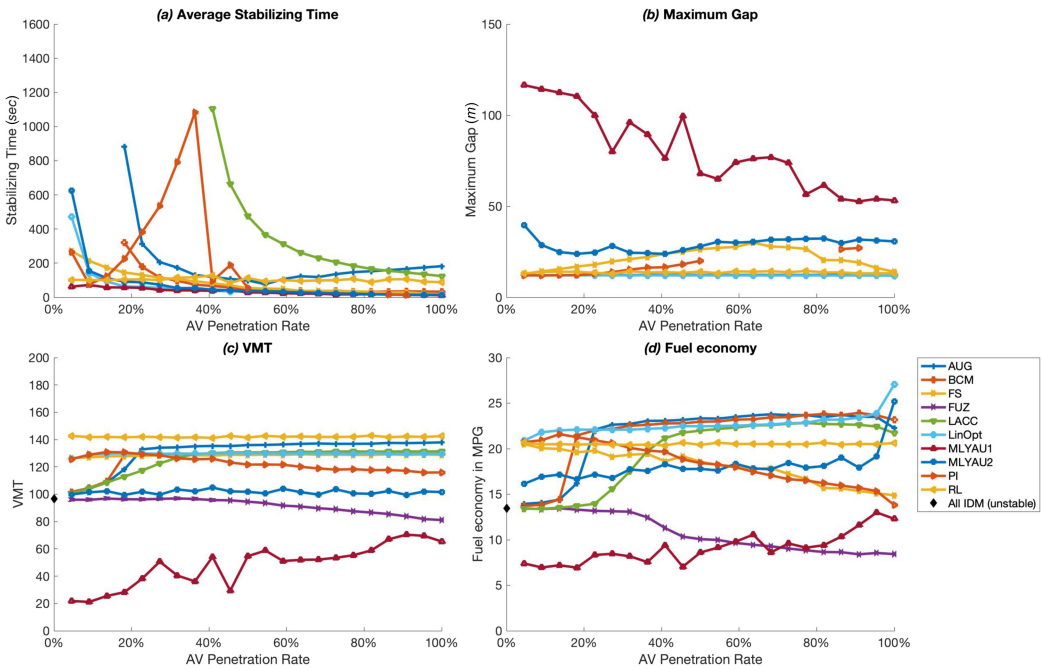


Fig. 5. Time to stabilize (a), maximum final gap (b), VMT (c), and fuel economy (d) for the clustered case scenario. For (c) and (d), black dots are the baseline scenario values, where all vehicles are HVs.

penetration rates (e.g., AUG, BCM, LACC). There are two exceptions in which the fuel economy is getting worse at higher penetration rates: FS and PI. For PI, as we have seen, the stability is getting worse at higher penetration rates; hence, the fuel economy is also getting worse at higher penetration rates. It is interesting to note that the fuel economy of FS also gets worse even though the traffic flow is getting smoother. The possible reason is that FS is actually doing a lot of subtle acceleration and deceleration. This is because FS is essentially a speed controller, and the process of converting speed command to acceleration introduces “noise” into the acceleration command, which causes higher fuel consumption.

3.4.2 Scenario II. Results of scenario II are presented in this section. Similar to the previous section, for scenario II, the corresponding values when the traffic on the ring is stable are presented in Table 7. In this scenario, the penetration rate is only limited to about 9% to 50% of AV penetration in the system given that the placement of the AVs has to follow an even distribution (as shown in Table 5).

From Table 7, we can see that the overall results appear to be similar to scenario I with minimal changes in the values. Again, it failed to stabilize when FUZ is used. It takes the most number of AVs for LACC to work, whereas the number of AUG needs to be increased to 6 from 3 and the number of BCM needs to be increased to 5 from 3 in scenario I for the system to be stable.

To further differentiate the controllers based on their performance at different penetration rates, results across different penetration rates also presented in Figure 6. Again, we can see the same trend as in the previous scenario if we look at Figure 6(a) where the time to stabilize for the ring generally decreases as the AV penetration rate increases, except for PI, where it also could get unstable at high penetration rates. In Figure 6(b), we can restate our prior observations that the

Table 7. Average Performance Comparison of Scenario II: Evenly Distributed

Controller	Minimum No. of AVs to Stabilize	Time to Stabilize (in seconds)	Max Gap (in meters)	VMT	Fuel Economy (in miles per gallon)
AUG	6	272.04	12.19	133.83	22.28
BCM	5	1516.9	12.29	127.06	19.32
FS	1	196.23	12.70	127.17	20.18
FUZ	Unstable	N/A	N/A	N/A	N/A
LACC	9	1,213.55	12.13	129.98	21.05
LinOpt	1	120.50	12.12	128.99	21.82
MLYAU1	1	61.41	114.97	24.27	7.70
MLYAU2	1	151.23	36.87	101.13	16.82
PI	1	86.98	12.01	128.69	21.13
RL	1	241.03	14.52	138.69	19.70

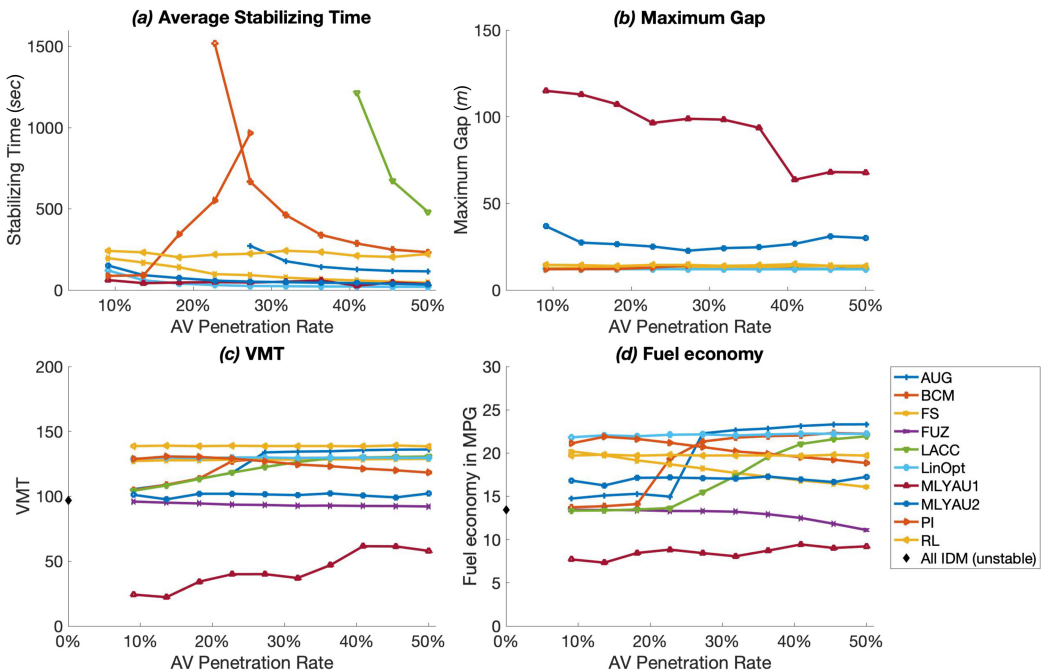


Fig. 6. Time to stabilize (a), maximum final gap (b), VMT (c), and fuel economy (d) for the evenly distributed scenario. For (c) and (d), black dots are the baseline scenario values, where all vehicles are HVs.

maximum gap is invariant with respect to the penetration rate except for the two Lyapunov-based controllers for the same reasons mentioned previously. In Figure 6(c) and (d), the trends of VMT and fuel economy are also similar to the previous scenario.

3.4.3 Comparison Across Two Scenarios. To further compare the influences of distributions of AVs, Figure 7 through Figure 10 arrange the results in a different way. We overlay the results of different scenarios on top of each scenario for different types of AVs. Figure 7 shows the time to stabilize for each AV. For most of the AVs, the time to stabilize is decreasing with an increasing penetration rate or kept the same. However, PI shows that as the penetration rate increases, traffic

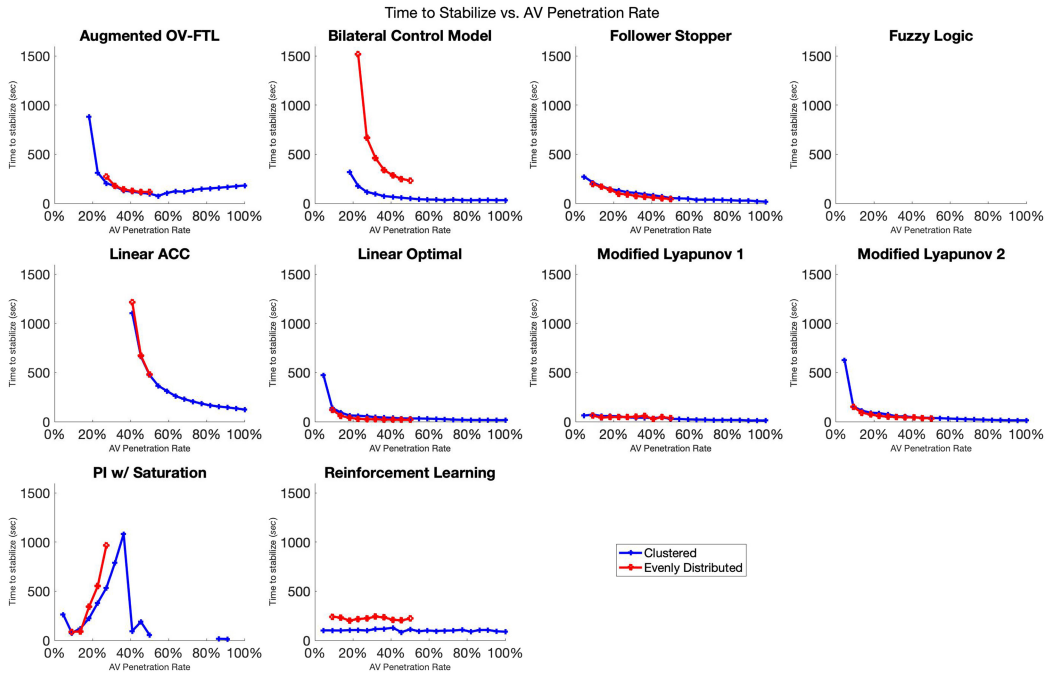


Fig. 7. Time to stabilize the ring road for AV controllers under different penetration rates and different distributions.

becomes less stable. This may imply that PI is more appropriate when AV penetration rate is low. For most of the AVs, it can be noted that variation of the stabilizing time is not significant across different AV distributions, whereas it is more relevant to AV types and the penetration rate. BCM shows a significant difference between two distributions. The performance of BCM is much better when they are clustered together than being separated.

Figure 8 shows the maximum gap for each AV. Only the results of FS show that the maximum gap is a little shorter in the case of the evenly distributed scenario. There is no significant discrepancy for other type of AVs.

Figure 9 shows the VMT for each AV. The VMT is also not sensitive to the variation of AV distributions. With the help of AVs smoothing traffic flow, the VMTs are significantly increased compared to the baseline case, except for FUZ and MLYAU1. FUZ results in slightly lower VMT because it was not able to stabilize the traffic flow under any penetration rate. MLYAU1 stops the traffic, so the VMT is much smaller than the baseline. Figure 10 shows the fuel economy for each AV. For AVs, fuel economy does not show much change with the change in penetration rates and AV distributions.

4 CONCLUSION

In this article, AVs dissipating stop-and-go waves on a ring road are studied under different distributions and penetration rates. To evaluate their performance, experiments are carried out in a state-of-the-art simulation framework. Our findings are summarized as follows:

- Out of 10 AVs, 6 AV models are able to stabilize the ring road traffic at a penetration rate as low as 5%. They are FS, LinOpt, MLYAU1, MLYAU2, PI, and RL.

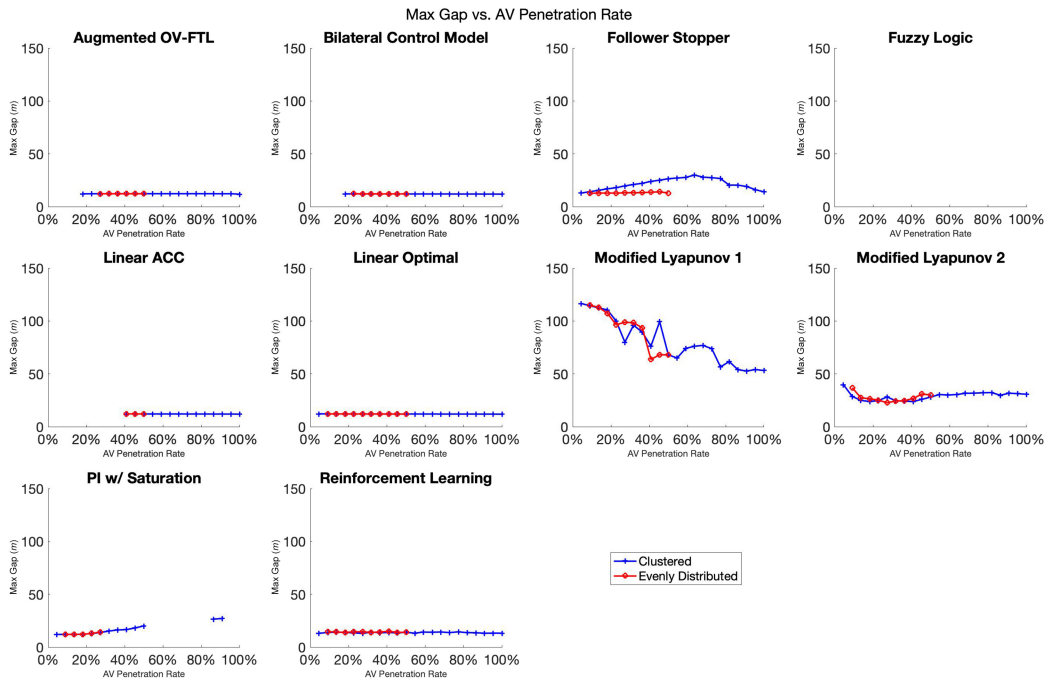


Fig. 8. Maximum gap for AV controllers under different penetration rates and different distributions.

- In general, the stabilizing time is shorter if more AVs are placed in the traffic. However, for PI, the performance is degraded when more AVs are placed.
- FUZ is the only controller that is not able to meet stability based on the set criterion, but it is able to ensure that the traffic moves on the ring without encountering any vehicular crashes.
- The RL controller shows the most consistent traffic improvement under all circumstances for all four metrics. It shows more than 40% VMT improvement while maintaining good fuel economy.
- MLYAU1 stabilizes the ring road with a trivial speed, where it almost stops all the vehicles in the system.
- For most of the AVs, the performance of the AVs is not much related to the way they are distributed among the traffic (except PI and BCM). No matter whether they are clustered (i.e., platooned) or evenly distributed, the performance of AVs is pretty much the same. However, this shall be treated with a caveat. This might only be applicable when we treat control of AVs individually (i.e., no cooperation/communication among them), as a recent study by Li et al. [19] mentions that the distribution of AVs may have a big impact when we consider the cooperation of multiple AVs.
- PI is one of the two controllers that shows some difference between two distributions. It is interesting to see that the performance of PI is not as good as in the *clustered* case compared to being *evenly distributed*. When PI is placed in the manner of scenario II, the performance of PI is degraded severely as multiple AVs are placed in the traffic.
- Another controller that shows quite different results for different distributions is BCM. The results of the time to stabilize also show that it performs better under a clustered scenario.

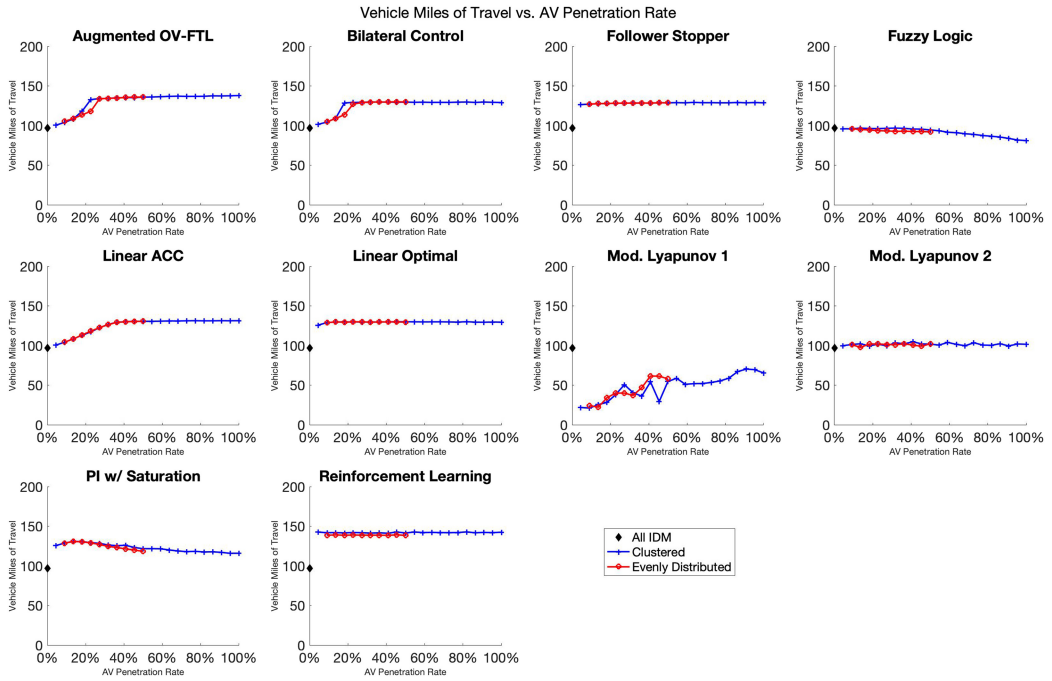


Fig. 9. VMT for AV controllers under different penetration rates and different distributions. The baseline VMT is 96.71.

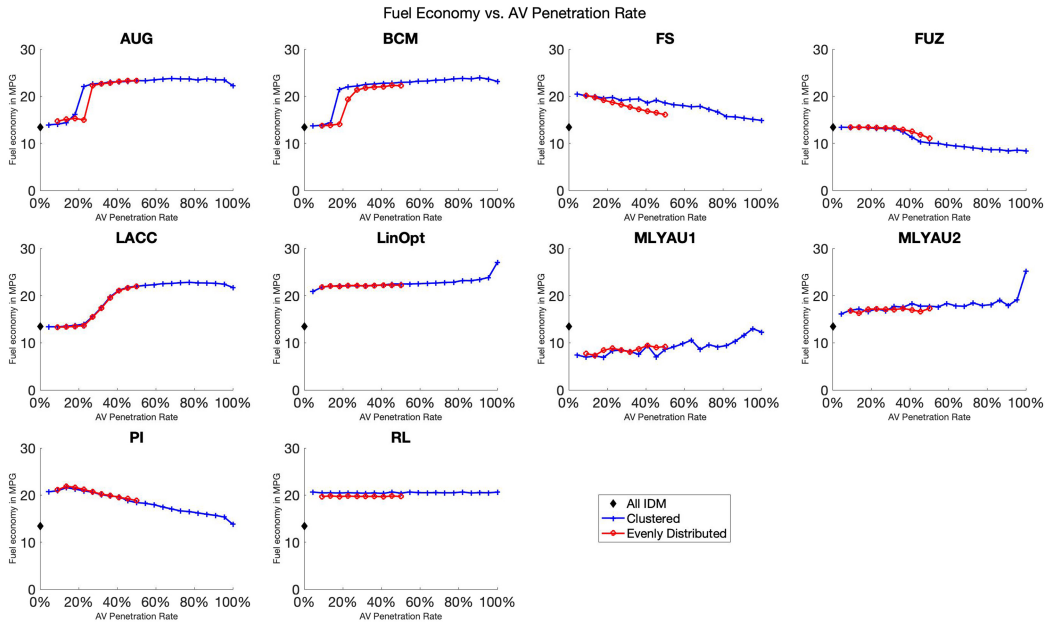


Fig. 10. Fuel economy in miles per gallon under different penetration rates and different distributions. The baseline fuel economy is 13.12 miles per gallon.

APPENDIX

A NUMBER OF UNSTABLE RUNS

Disclaimer: Because of the randomness, for a few of the controllers, some of the stable (or unstable) results are not 100% reproducible. In other words, for a few AVs, under the same distribution and the same penetration rate, the simulations may not always become stable (or unstable). For those marginal cases, we say they are stable if more than 50% of the simulation runs are stable.

Table 8. Number of Unstable Runs (Out of 10): Clustered

Penetration Rate (%)	AUG	BCM	FS	FUZ	LACC	LinOpt	MLYAU1	MLYAU2	PI	RL
4.55	10	10	0	10	10	0	0	0	1	0
9.09	10	10	0	10	10	0	0	0	0	0
13.64	7	10	0	10	10	0	0	0	0	0
18.18	0	0	0	10	10	0	0	0	0	0
22.73	0	0	0	10	10	0	0	0	0	0
27.27	0	0	0	10	10	0	0	0	0	0
31.82	0	0	0	10	10	0	0	0	0	0
36.36	0	0	0	10	10	0	0	0	1	0
40.91	0	0	0	10	0	0	0	0	8	0
45.45	0	0	0	10	0	0	0	0	9	0
50.00	0	0	0	10	0	0	0	0	9	0
54.55	0	0	0	10	0	0	0	0	10	0
59.09	0	0	0	10	0	0	0	0	10	0
63.64	0	0	0	10	0	0	0	0	10	0
68.18	0	0	0	10	0	0	0	0	10	0
72.73	0	0	0	10	0	0	0	0	10	0
77.27	0	0	0	10	0	0	0	0	10	0
81.82	0	0	0	10	0	0	0	0	10	0
86.36	0	0	0	10	0	0	0	0	9	0
90.91	0	0	0	10	0	0	0	0	6	0
95.45	0	0	0	10	0	0	0	0	10	0
100.00	0	0	0	10	0	0	0	0	10	0

Table 9. Number of Unstable Runs (Out of 10): Evenly Distributed

Penetration Rate (%)	AUG	BCM	FS	FUZ	LACC	LinOpt	MLYAU1	MLYAU2	PI	RL
9.09	10	10	0	10	10	0	0	0	0	0
13.64	10	10	0	10	10	0	0	0	0	0
18.18	10	10	0	10	10	0	0	0	0	0
22.73	10	5	0	10	10	0	0	0	0	0
27.27	0	0	0	10	10	0	0	0	0	0
31.82	0	0	0	10	10	0	0	0	10	0
36.36	0	0	0	10	10	0	0	0	10	0
40.91	0	0	0	10	0	0	0	0	10	0
45.45	0	0	0	10	0	0	0	0	10	0
50.00	0	0	0	10	0	0	0	0	10	0

ACKNOWLEDGMENTS

The authors would like to thank Jonathan Lee for providing valuable comments for this work. The authors would also like to acknowledge Yousef Ballout for his help in running a few of initial simulations; Ashkan Yousefpour, Alexander Keimer, Nishant Kheterpal, and Fangyu Wu for their technical support; Kanaad Parvate and Daniel B. Work for sharing references; and Joy Carpio for sharing comments at an earlier stage of this work. A. R. Bagabaldo is thankful for the Philippine CHED, DOST-SEI, and Mapua University for his Ph.D. scholarship.

REFERENCES

- [1] Assad Alam, Bart Besselink, Valerio Turri, Jonas Martensson, and Karl H. Johansson. 2015. Heavy-duty vehicle platooning for sustainable freight transportation: A cooperative method to enhance safety and efficiency. *IEEE Control Systems* 35, 6 (2015), 34–56.
- [2] Masako Bando, Katsuya Hasebe, Akihiro Nakayama, Akihiro Shibata, and Yuki Sugiyama. 1994. Structure stability of congestion in traffic dynamics. *Japan Journal of Industrial and Applied Mathematics* 11, 2 (1994), 203.
- [3] Masako Bando, Katsuya Hasebe, Akihiro Nakayama, Akihiro Shibata, and Yuki Sugiyama. 1995. Dynamical model of traffic congestion and numerical simulation. *Physical Review E* 51, 2 (1995), 1035.
- [4] Mark Brackstone and Mike McDonald. 1999. Car-following: A historical review. *Transportation Research Part F: Traffic Psychology and Behaviour* 2, 4 (Dec. 1999), 181–196. [https://doi.org/10.1016/S1369-8478\(00\)00005-X](https://doi.org/10.1016/S1369-8478(00)00005-X)
- [5] Fang-Chieh Chou, Hani Ramezani, Xiao-Yun Lu, Steven E. Shladover, and Osman D. Altan. 2018. Modeling vehicle-following dynamics of heavy trucks under automatic speed control based on experimental data. In *Proceedings of the Transportation Research Board 97th Annual Meeting*.
- [6] Shumo Cui, Benjamin Seibold, Raphael Stern, and Daniel B. Work. 2017. Stabilizing traffic flow via a single autonomous vehicle: Possibilities and limitations. In *Proceedings of the 2017 IEEE Intelligent Vehicles Symposium (IV'17)*. IEEE, Los Alamitos, CA, 1336–1341.
- [7] L. C. Davis. 2004. Effect of adaptive cruise control systems on traffic flow. *Physical Review E* 69, 6 (June 2004), 066110. <https://doi.org/10.1103/PhysRevE.69.066110>
- [8] Maria Laura Delle Monache, Thibault Liard, Anais Rat, Raphael Stern, Rahul Badhani, Benjamin Seibold, Jonathan Sprinkle, Daniel Work, and Benedetto Piccoli. 2019. Feedback control algorithms for the dissipation of traffic waves with autonomous vehicles. In *Computational Intelligence and Optimization Methods for Control Engineering*. Springer, 1–20. <https://hal.inria.fr/hal-01930724>.
- [9] Yan Duan, Xi Chen, Rein Houthoofd, John Schulman, and Pieter Abbeel. 2016. Benchmarking deep reinforcement learning for continuous control. arXiv:1604.06778 [cs.LG].
- [10] R. Firoozi, S. Nazari, J. Guanetti, R. O’Gorman, and F. Borrelli. 2019. Safe adaptive cruise control with road grade preview and V2V communication. In *Proceedings of the 2019 American Control Conference (ACC'19)*. 4448–4453.
- [11] Jin I. Ge and Gábor Orosz. 2014. Dynamics of connected vehicle systems with delayed acceleration feedback. *Transportation Research Part C: Emerging Technologies* 46 (2014), 46–64. <https://doi.org/10.1016/j.trc.2014.04.014>
- [12] Tuomas Haarnoja, Aurick Zhou, Pieter Abbeel, and Sergey Levine. 2018. Soft actor-critic: Off-policy maximum entropy deep reinforcement learning with a stochastic actor. In *Proceedings of the 35th International Conference on Machine Learning*. <http://arxiv.org/abs/1801.01290>.
- [13] R’mani Haulcy, Nathaniel Hamilton, Rahul Bhadani, Jonathan Sprinkle, Daniel B. Work, Nathalie Rizzo, Benedetto Piccoli, Maria Laura Delle Monache, and Benjamin Seibold. 2017. A Fuzzy-Based Approach to Dampen Emergent Traffic Waves. Retrieved November 23, 2021 from https://www.csl.uawebhost.arizona.edu/sites/default/files/A_Fuzzy_based_approach_to_Dampen_Emergent_Traffic_Waves.pdf.
- [14] Robert Herman, Elliott W. Montroll, Renfrey B. Potts, and Richard W. Rothery. 1959. Traffic dynamics: Analysis of stability in car following. *Operations Research* 7, 1 (1959), 86–106. <https://doi.org/10.1287/opre.7.1.86>
- [15] Berthold K. P. Horn. 2013. Suppressing traffic flow instabilities. In *Proceedings of the 16th International IEEE Conference on Intelligent Transportation Systems (ITSC'13)*. 13–20. <https://doi.org/10.1109/ITSC.2013.6728204>
- [16] Berthold K. P. Horn and Liang Wang. 2017. Wave equation of suppressed traffic flow instabilities. *IEEE Transactions on Intelligent Transportation Systems* 99 (2017), 1–10.
- [17] E. Kometani and T. Sasaki. 1959. Dynamic behavior of traffic with a nonlinear spacing-speed relationship. In *Proceedings of the Symposium on Theory of Traffic Flow*. 105–119.
- [18] Abdul Rahman Kreidieh, Cathy Wu, and Alexandre M. Bayen. 2018. Dissipating stop-and-go waves in closed and open networks via deep reinforcement learning. In *Proceedings of the IEEE Conference on Intelligent Transportation Systems (ITSC'18)*. 1475–1480. <https://doi.org/10.1109/ITSC.2018.8569485>
- [19] Keqiang Li, Jiawei Wang, and Yang Zheng. 2020. Cooperative formation of autonomous vehicles in mixed traffic flow: Beyond platooning. arXiv:2009.04254 [eess.SY].
- [20] Chi-Ying Liang and Huei Peng. 1999. Optimal adaptive cruise control with guaranteed string stability. *Vehicle System Dynamics* 32, 4–5 (1999), 313–330.
- [21] Eric Liang, Richard Liaw, Robert Nishihara, Philipp Moritz, Roy Fox, Ken Goldberg, Joseph E. Gonzalez, Michael I. Jordan, and Ion Stoica. 2018. RLlib: Abstractions for distributed reinforcement learning. In *Proceedings of the International Conference on Machine Learning (ICML'18)*.
- [22] Hao Liu, Xingan (David) Kan, Steven E. Shladover, Xiao-Yun Lu, and Robert E. Ferlis. 2018. Impact of cooperative adaptive cruise control on multilane freeway merge capacity. *Journal of Intelligent Transportation Systems* 22, 3 (2018), 263–275. <https://doi.org/10.1080/15472450.2018.1438275>

- [23] Pablo Alvarez Lopez, Michael Behrisch, Laura Bieker-Walz, Jakob Erdmann, Yun-Pang Flötteröd, Robert Hilbrich, Leonhard Lücken, Johannes Rummel, Peter Wagner, and Evamarie Wießner. 2018. Microscopic traffic simulation using SUMO. In *Proceedings of the IEEE Intelligent Transportation Systems Conference (ITSC'18)*. <https://elib.dlr.de/124092/>.
- [24] Silvia Magdici and Matthias Althoff. 2017. Adaptive cruise control with safety guarantees for autonomous vehicles. *IFAC-PapersOnLine* 50, 1 (2017), 5774–5781. <https://doi.org/10.1016/j.ifacol.2017.08.418> 20th IFAC World Congress.
- [25] Vicente Milanés and Steven E. Shladover. 2014. Modeling cooperative and autonomous adaptive cruise control dynamic responses using experimental data. *Transportation Research Part C: Emerging Technologies* 48 (2014), 285–300.
- [26] Kai Nagel and Michael Schreckenberg. 1992. A cellular automaton model for freeway traffic. *Journal de Physique I* 2, 12 (1992), 2221–2229.
- [27] G. F. Newell. 2002. A simplified car-following theory: A lower order model. *Transportation Research Part B: Methodological* 36, 3 (2002), 195–205. [https://doi.org/10.1016/S0191-2615\(00\)00044-8](https://doi.org/10.1016/S0191-2615(00)00044-8)
- [28] Gábor Orosz, R. Eddie Wilson, and Gabor Stefan. 2010. Traffic jams: Dynamics and control. *Philosophical Transactions of the Royal Society A: Mathematical, Physical and Engineering Sciences* 368, 1928 (2010), 4455–4479. <https://doi.org/10.1098/rsta.2010.0205>
- [29] L. A. Pipes. 1953. An operational analysis of traffic dynamics. *Journal of Applied Physics* 41 (1953), 274–281.
- [30] Rajesh Rajamani. 2011. *Vehicle Dynamics and Control*. Springer Science & Business Media.
- [31] Hani Ramezani, Steven E. Shladover, Xiao-Yun Lu, and Osman D. Altan. 2018. Micro-simulation of truck platooning with cooperative adaptive cruise control: Model development and a case study. *Transportation Research Record* 2672, 19 (2018), 55–65. <https://doi.org/10.1177/0361198118793257> arXiv:<https://doi.org/10.1177/0361198118793257>
- [32] A. Reuschel. 1950. Fahrzeugbewegungen in der kolonne. *Österreichisches Ingenieur-Archiv* 4, 3-4 (1950), 193–215.
- [33] John Schulman, Filip Wolski, Prafulla Dhariwal, Alec Radford, and Oleg Klimov. 2017. Proximal policy optimization algorithms. arXiv:[1707.06347](https://arxiv.org/abs/1707.06347).
- [34] Raphael E. Stern, Shumo Cui, Maria Laura Delle Monache, Rahul Bhadani, Matt Bunting, Miles Churchill, Nathaniel Hamilton, et al. 2018. Dissipation of stop-and-go waves via control of autonomous vehicles: Field experiments. *Transportation Research Part C: Emerging Technologies* 89 (Feb. 2018), 205–221. <https://doi.org/10.1016/j.trc.2018.02.005> arXiv:[1705.01693](https://arxiv.org/abs/1705.01693)
- [35] Yuki Sugiyama, Minoru Fukui, Macoto Kikuchi, Katsuya Hasebe, Akihiro Nakayama, Katsuhiro Nishinari, Shin Ichi Tadaki, and Satoshi Yukawa. 2008. Traffic jams without bottlenecks experimental evidence for the physical mechanism of the formation of a jam. *New Journal of Physics* 10, 3 (2008), 033001.
- [36] Richard S. Sutton and Andrew G. Barto. 1998. *Introduction to Reinforcement Learning*. MIT Press, Cambridge, MA.
- [37] Shin Ichi Tadaki, Macoto Kikuchi, Minoru Fukui, Akihiro Nakayama, Katsuhiro Nishinari, Akihiro Shibata, Yuki Sugiyama, Taturu Yosida, and Satoshi Yukawa. 2013. Phase transition in traffic jam experiment on a circuit. *New Journal of Physics* 15 (2013), 103034. <https://doi.org/10.1088/1367-2630/15/10/103034>
- [38] J. R. R. Tolkien. 1954. *The Lord of the Rings*. Ballantine Books, New York, NY.
- [39] Martin Treiber, Ansgar Hennecke, and Dirk Helbing. 2000. Congested traffic states in empirical observations and microscopic simulations. *Physical Review E* 62, 2 (Aug. 2000), 1805–1824. <https://doi.org/10.1103/PhysRevE.62.1805>
- [40] Martin Treiber and Arne Kesting. 2013. *Traffic Flow Dynamics*. Springer. <https://doi.org/10.1007/978-3-642-32460-4>
- [41] Valerio Turri, Yeojun Kim, Jacopo Guanetti, Karl H. Johansson, and Francesco Borrelli. 2017. A model predictive controller for non-cooperative eco-platooning. In *Proceedings of the 2017 IEEE American Control Conference (ACC'17)*. IEEE, Los Alamitos, CA, 2309–2314.
- [42] Willem van Willigen, Leon Kester, Ellen van Nunen, and Evert Haasdijk. 2015. Safety in the face of uncertainty: Critical headway estimation in cooperative adaptive cruise control. *International Journal of Intelligent Transportation Systems Research* 13 (2015), 95–106.
- [43] Jiawei Wang, Yang Zheng, Chaoyi Chen, Qing Xu, and Keqiang Li. 2020. Leading cruise control in mixed traffic flow. arXiv:[2007.11753](https://arxiv.org/abs/2007.11753)
- [44] J. Wang, Y. Zheng, Q. Xu, J. Wang, and K. Li. 2020. Controllability analysis and optimal control of mixed traffic flow with human-driven and autonomous vehicles. *IEEE Transactions on Intelligent Transportation Systems* PP, 99 (2020), 1–15. <https://doi.org/10.1109/TITS.2020.3002965>
- [45] L. Wang and B. K. P. Horn. 2020. On the chain stability of bilateral control model. *IEEE Transactions on Automatic Control* 65, 8 (2020), 3397–3408. <https://doi.org/10.1109/TAC.2019.2945877>
- [46] C. Wu, A. M. Bayen, and A. Mehta. 2018. Stabilizing traffic with autonomous vehicles. In *Proceedings of the 2018 IEEE International Conference on Robotics and Automation (ICRA'18)*. 6012–6018. <https://doi.org/10.1109/ICRA.2018.8460567>
- [47] Cathy Wu, Aboudy Kreidieh, Kanaad Parvate, Eugene Vinitzky, and Alexandre M. Bayen. 2017. Flow: Architecture and benchmarking for reinforcement learning in traffic control. arXiv:[1710.05465](https://arxiv.org/abs/1710.05465).

- [48] Cathy Wu, Aboudy Kreidieh, Kanaad Parvate, Eugene Vinitzky, and Alexandre M. Bayen. 2019. Flow: A modular learning framework for autonomy in traffic. arXiv:1710.05465 [cs.AI]
- [49] C. Wu, K. Parvate, N. Kheterpal, L. Dickstein, A. Mehta, E. Vinitzky, and A. M. Bayen. 2017. Framework for control and deep reinforcement learning in traffic. In *Proceedings of the 2017 IEEE 20th International Conference on Intelligent Transportation Systems (ITSC'17)*. 1–8. <https://doi.org/10.1109/ITSC.2017.8317694>
- [50] Fangyu Wu, Raphael E. Stern, Shumo Cui, Maria Laura Delle Monache, Rahul Bhadani, Matt Bunting, Miles Churchill, et al. 2019. Tracking vehicle trajectories and fuel rates in phantom traffic jams: Methodology and data. *Transportation Research Part C: Emerging Technologies* 99 (July 2019), 82–109. <https://doi.org/10.1016/j.trc.2018.12.012>
- [51] D. Xie, X. Zhao, and Z. He. 2019. Heterogeneous traffic mixing regular and connected vehicles: Modeling and stabilization. *IEEE Transactions on Intelligent Transportation Systems* 20, 6 (2019), 2060–2071. <https://doi.org/10.1109/TITS.2018.2857465>
- [52] Diana Yanakiev and Ioannis Kanellakopoulos. 1996. Speed tracking and vehicle follower control design for heavy-duty vehicles. *Vehicle System Dynamics* 25, 4 (1996), 251–276.
- [53] Yang Zheng, Jiawei Wang, and Keqiang Li. 2018. Smoothing traffic flow via control of autonomous vehicles. arXiv:1812.09544v1.

Received October 2020; revised March 2021; accepted October 2021